Entangled Nematic Colloidal Dimers and Wires

M. Ravnik,[1] M. Škarabot,[2] S. Žumer,[1,2] U. Tkalec,[2] I. Poberaj,[1] D. Babič,[1] N. Osterman,[1] and I. Muševič[1,2,*]

[1]*Faculty of Mathematics and Physics, University of Ljubljana, Jadranska 19, 1000 Ljubljana, Slovenia*

[2]*J. Stefan Institute, Jamova 39, 1000 Ljubljana, Slovenia*

(Received 20 June 2007; published 12 December 2007)

It has been predicted, but never confirmed, that colloidal particles in a nematic liquid crystal could be self-assembled by delocalized topological defects and entangled disclinations. We show experimentally and theoretically that colloidal dimers and 1D structures bound by entangled topological defect loops can indeed be created by locally thermally quenching a thin layer of the nematic liquid crystal around selected colloidal particles. The topological entanglement provides a strong stringlike binding, which is ten thousand times stronger compared to water-based colloids. This unique binding mechanism could be used to assemble resonator optical waveguides and robust chiral and achiral structures of topologically entangled colloids that we call colloidal wires.

DOI: 10.1103/PhysRevLett.99.247801 PACS numbers: 61.30.Jf, 47.57.J−, 83.10.Pp

The capacity to generate predetermined spatial arrangements of particles on different length scales is one of the central issues of nanotechnology. Current concepts rely on single atom and molecule manipulation by the sharp tip of the STM [1], particle manipulation by the laser or optoelectronic tweezers [2–4], microfluidics, and optofluidics [5], and micromanipulation in combination with lithography [6]. Of particular importance is 3D self-assembly, where the spatial arrangements of particles, such as photonic crystals, could be realized spontaneously [7].

Dispersions of colloidal particles in the nematic liquid crystals show an amazing diversity of patterns, such as chains [8] and 2D colloidal crystals [9], which are assembled by topological defects [10], which mediate the elastic distortion forces between the colloidal inclusions [11–14]. Recently, it has been predicted, that colloidal particles in the nematic liquid crystal could be assembled by delocalized defects [15] or entangled topological defects in a form of single closed defect loops, extending over several colloidal particles [16,17]. In this case, one or several defect lines entangle two or many colloidal particles, which gives rise to binding forces between the particles. Although primarily elastic in origin, these binding forces are a direct consequence of the nontrivial topology of the entangled director field, and can thus be considered as topological in nature.

Here we show experimentally and theoretically, that colloidal dimers and wires can be assembled by entangled topological loops of the nematic orientational field. We have found that the colloidal entanglement proceeds exclusively via locally thermally quenching a thin layer of the nematic liquid crystal around selected colloidal particles, which explains why the entanglement has not been observed before. Three linear entangled defect structures have been found experimentally, which are topologically equivalent, but differ in the way of binding and in the particle separation. In all cases, the entanglement provides ten thousand times stronger binding compared to water-based colloids.

Following predictions of colloidal structures entangled by disclination lines [16,17] or delocalized defects [15], we have performed the experiments in nematic colloids, confined to thin planar cells of thickness from 5 to 22 μm, which provided a homogeneous orientation of the nematic liquid crystal pentylcyanobiphenyl (5CB) inside the measuring cell. The surfaces of the colloidal particles (glass microspheres of diameter 4.7 and 19 μm) were treated chemically to induce local perpendicular alignment of liquid crystal molecules [18]. In a thin layer, the nematic liquid crystal around the colloidal particles adopts the ''Saturn ring'' configuration [9,19], where the topological defect in a form of a defect ring with the winding number $-1/2$ [11,12] encircles the particle and carries the topological charge -1.

We have used the laser tweezers to manipulate and assemble colloidal particles in a liquid crystal. Using a high intensity laser beam, we have heated the liquid crystal locally around the selected colloidal particles into the isotropic phase, and quenched it into the nematic phase by switching-off the light. Figure 1(a) presents the time sequence of unpolarized optical micrographs of the nematic liquid crystal around two 19 μm colloidal particles after quench. One can clearly see the formation of a single disclination loop out of dense tangle of topological defects. In a fraction of a second, the entangled topological defect encircled both particles in the form of a twisted loop, i.e., a ''figure eight'' [17]. Two other types of binding were observed in the experiments. Figure 1(c) presents the formation of a more complicated, asymmetrically entangled single disclination loop, which we call the ''figure of omega.'' In contrast to the figure of eight shown in Fig. 1(a), the figure of omega has a straight defect line at the front side, which sinks behind both colloidal particles and makes an additional loop in between them. In most of the experiments, this configuration is unstable and transforms slowly into another more stable configuration, shown in Fig. 1(d). Here, the final colloidal separation is large, indicating a topological defect in between the

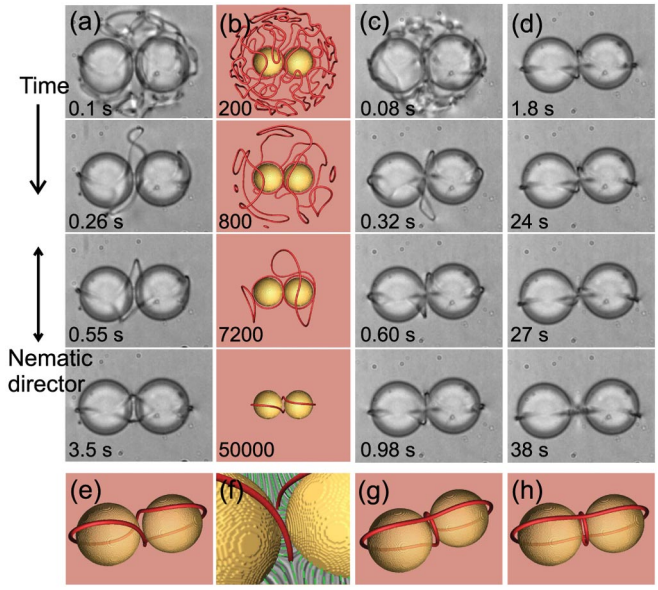

FIG. 1 (color). Assembling entangled colloidal pairs by thermal quench using light. The diameter of the particles is 19 μm, the cell thickness is 21 μm. (a) Figure of eight entangled state. The disclination loops are visible under a nonpolarizing optical microscope due to the scattering of light. (b) Numerical simulation of the time evolution of entanglement, measured in the number of iteration steps. Defects are represented by drawing the surfaces of constant order parameter S (colored red, corresponding to $S = 0.5$). (c) Evolution of the figure of omega entangled state. (d) The figure of omega was unstable and transformed into the entangled hyperbolic defect. (e) The calculated figure of eight structure. (f) Close-up look at the director field in the gap between the microspheres for the figure of eight. (g) Calculated figure of omega structure. (h) Calculated entangled hyperbolic defect structure.

spheres. We call it the ''entangled hyperbolic defect'' structure. In total of 124 quenching experiments, 52% of the final states were entangled, the rest was not entangled. 36% of the states were figure of eight, 13% were figure of omega, and only 3% were entangled hyperbolic point defect states.

The details of these colloidal dimers were revealed by numerically analyzing the creation process of the entangled colloidal states using Landau–de Gennes (LdG) approach [20]. It is based on the tensorial order parameter Q_{ij} describing the local collective orientation of the liquid crystalline molecules along the director, the degree of their local ordering and possible biaxality of the distribution. The free energy F of a nematic liquid crystal in a single elastic constant approximation [20] is

$$F = +\frac{1}{2}L\int_{LC}\left(\frac{\partial Q_{ij}}{\partial x_k}\right)\left(\frac{\partial Q_{ij}}{\partial x_k}\right)dV + \int_{LC}\left(\frac{1}{2}AQ_{ij}Q_{ji} + \frac{1}{3}BQ_{ij}Q_{jk}Q_{ki} + \frac{1}{4}C(Q_{ij}Q_{ji})^2\right)dV + \frac{1}{2}W\int_{\text{Surf.Col.}}(Q_{ij} - Q^0_{ij})(Q_{ji} - Q^0_{ji})dS. \quad (1)$$

Here the summation over repeated indices is assumed, L is the elastic constant, A, B, and C are the nematic material constants, W is the strength of the surface anchoring, and Q^0_{ij} describes the preferable surface order and orientation. The following parameter values were used: $A = -0.172 \times 10^6$ J/m^3, $B = -2.12 \times 10^6$ J/m^3, $C = 1.73 \times 10^6$ J/m^3, $W = 1 \times 10^{-2}$ J/m^2, the cell thickness 2 μm, the particle diameter $d = 1$ μm, and $L = 4 \times 10^{-11}$ N. The equilibrium tensorial order parameter field, which describes the local average orientations of liquid crystal molecules, and therefore also the defect structure, was found by solving a set of coupled nonlinear partial differential equations, obtained by minimizing the free energy F with proper boundary conditions. An explicit Euler relaxation algorithm on a cubic mesh [21] was used and the relaxation procedure was performed in two stages. First, the order parameter tensor profile for chosen particle positions was determined via minimization of the free energy. Then, the free energy was further minimized via systematic reposition of particles. The relaxation procedure was stopped when the free energy changes dropped below ~0.01%.

The number of possible metastable states increases with the complexity of the confinement. We have therefore decided to explore these possible states by starting our relaxation from the isotropic phase. This means that initial director at each mesh point was generated by a random process which allowed us that by repeating the procedure possible local minima of the free energy were found automatically. The similarity between the ''numerical relaxation experiment'' shown in Fig. 1(b) and the real experiment [Fig. 1(a)] is striking, showing the inherent power of our procedure based on the LdG approach. When numerically quenching the system first a large number of defect lines have formed, which relaxed via shrinking, merging and annihilation. Just like in the real experiment the defect lines condensed around two particles either in a form of separate Saturn rings, or in a form of more complex $-1/2$ defect lines, entangling the pair [Figs. 1(e), 1(g), and 1(h)]. Three local minima in the free energy corresponding to three experimentally observed entangled structures were found: figure of eight [Figs. 1(e) and 1(f)], figure of omega [Fig. 1(g)], and entangled hyperbolic defect [Fig. 1(h)]. The figure of eight is formed by a single twisted $-1/2$ defect line, encircling both colloidal particles. The structure is chiral, as the twist could be either left or right handed. The figure of omega colloidal pair is also a chiral object, as evident from Fig. 1(g). Finally, the entangled hyperbolic defect structure shown in Fig. 1(h) is nonchiral, as it is formed by two orthogonal, disconnected $-1/2$ defect loops.

The strength of the entanglement was measured by switching-on two separated light traps and grabbing two 4.7 μm microspheres at their opposite sides, as shown in Figs. 2(a) and 2(b). The entangled pair was stretched by moving both traps in the opposite direction to a predetermined position, and then the trap was switched off. The

time sequences in Figs. 2(a) and 2(b) show, that the entangled defect loop acts as an elastic string, pulling both colloidal particles together. Stringlike interaction between a pair of nematic colloidal particles was reported for other type of binding before [22,23]. From the recorded images, the effective force and the binding potential of the entangled line defects were determined as a function of separation [9], which is shown in Figs. 2(c) and 2(d). At larger separations, the stringlike force, corresponding roughly to the nematic deformation energy per unit length of a $-1/2$ disclination line, does not depend significantly on separation, and yields extremely strong effective inter-colloidal interaction, i.e., of the order of 10 000 of k_BT for 4.7 μm micro-spheres. The figure of eight loop breaks, if the separation is increased above a certain critical value of 7.5 μm for 4.7 μm spheres.

The corresponding calculated binding pair potentials are shown in Figs. 2(e) and 2(f). Whereas we observe good qualitative agreement between the theory and experiment for the ''figure of eight'' [Fig. 2(e)], the agreement is poor for the entangled point defect structure [Fig. 2(f)]. This is due to rather simple, single elastic constant approximation, used in the numerical calculations and also the sizes of the colloidal particles are quite different in the experiment and numerical analysis.

The free energy estimates based on the single elastic constant LdG approach indicate that all three entangled colloidal pairs are metastable with 0.3% (figure of eight), 0.9% (figure of omega and 0.7% (entangled hyperbolic defect) higher free energy compared to the free energy of a bound quadrupolar pair.

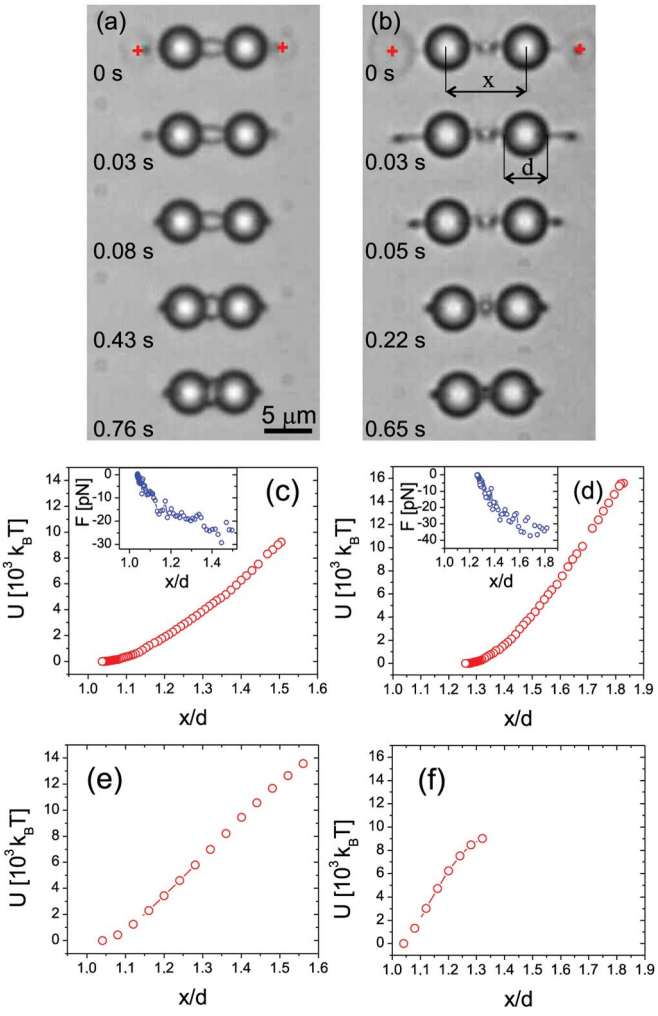

FIG. 2 (color). Stretching and releasing the topologically bound colloidal pair using light. (a) Using focused light of the laser tweezers (two red crosses on left and right), the figure of eight colloidal pair is first stretched and then released by switching-off the light. The diameter of the particles is 4.7 μm, the thickness of the cell is 6 μm. The force and the binding energy are calculated from the video frames (a), and shown in (c). (b) The same is done for entangled hyperbolic defects, shown in (d). (e) The pair binding energy, calculated for the figure of eight, as a function of particle separation x, normalized to the particle diameter d. (f) The pair binding energy, calculated for the entangled point defect as a function of separation x, normalized to the particle diameter d.

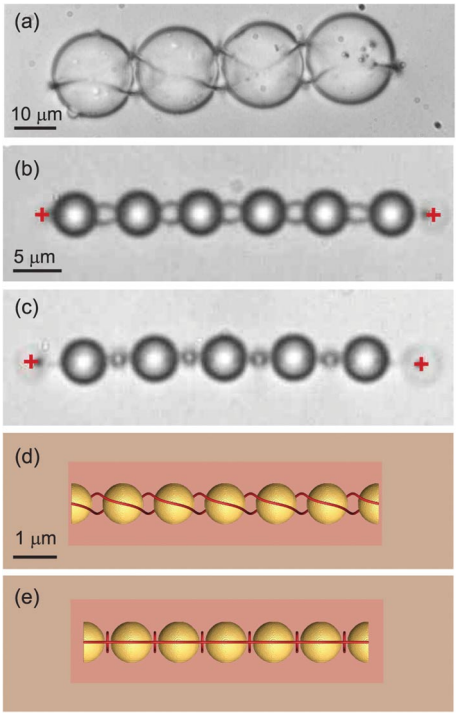

FIG. 3 (color). Colloidal wires assembled by entanglement. (a) Right-handed figure of eight colloidal wire assembled from 19 μm glass spheres. (b) Figure of eight colloidal wire made of 4.7 μm microspheres, stretched by light of the laser tweezers (red crosses). In the absence of light, the average equilibrium surface-surface separation between neighboring spheres is 160 nm. (c) Entangled hyperbolic defect colloidal wire, stretched by laser tweezers. Without light, the average equilibrium surface-surface separation between neighboring spheres is 1100 nm. (d) Calculated structure of stretched figure of eight colloidal wire. (e) Calculated structure of stretched entangled hyperbolic defect colloidal wire.

The entanglement is not necessarily limited only to colloidal pairs, but can extend over many colloidal particles, forming wires. Figures 3(a)–3(c) show colloidal wires, assembled by laser manipulation and thermal quenching. The colloidal wires in Figs. 3(a) and 3(b) are made of a chiral sequence of figure of eight loops and resemble a simple chiral braid, where two sides of a single connected defect line are winding along the colloidal particles. The third wire in Fig. 3(c) is nonchiral and is formed by a series of entangled hyperbolic defects. Both structures are in a good agreement with LdG simulation, shown in Figs. 3(d) and 3(e).

There are two important aspects of our work. First, we observe an interesting signature of the formation of entangled topological defects, as they can be created nearly exclusively by quenching from the isotropic phase. Whereas the conservation of the topological charge [24,25] assures that in our system the topological charge of defect loops is equal to the number of colloidal particles, it does not prescribe the nature of the loops. The formation of entangled defect loops is therefore ultimately connected to the symmetry breaking of the nematic orientational field across the isotropic-nematic phase transition, when a dense tangle of topological defects is formed after the quench through the Kibble mechanism [26]. Whereas in ''empty space'' these relics of the disordered phase annihilate after coarsening, in our case they condense at colloidal particles in a form of complicated nematic braids. This brings the underlying physics of our experiment into close relation to other observations of entanglement, such as the entanglement of vortices in superconductors [27] and superfluids [28], Alice strings [29], and cosmological Kibble mechanism of string formation [26]. The advantage is that we can study the entanglement in topologically nontrivial systems in real time and at micrometer scale.

Second, the observed strong binding of colloidal particles opens new routes to possible applications. We consider that by proper selection of materials, one could assemble closely spaced microresonator optical waveguides, which could transport light around sharp corners and kinks.

*Corresponding author.
igor.musevic@ijs.si

[1] G. Binnig and H. Rohrer, Helv. Phys. Acta **55**, 726 (1982).
[2] M. P. MacDonald, G. C. Spalding, and K. Dholakia, Nature (London) **426**, 421 (2003).
[3] D. G. Grier, Nature (London) **424**, 810 (2003).
[4] P. Yu Chiou, A. T. Ohta, and Ming C. Wu, Nature (London) **436**, 370 (2005).
[5] D. Psaltis, S. R. Quake, and C. Yang, Nature (London) **442**, 381 (2006).
[6] A. Aoki *et al.*, Nat. Mater. **2**, 117 (2003).
[7] V. W. A. de Villeneuve *et al.*, Science **309**, 1231 (2005); J. D. Joannopoulos, P. R. Villeneuve, and S. Fan, Nature (London) **386**, 143 (1997); A. van Blaaderen, R. Ruel, and P. Wiltzius, Nature (London) **385**, 321 (1997); Y. A. Vlasov, Xiang-Zheng Bo, J. C. Sturm, and D. J. Norris, Nature (London) **414**, 289 (2001); M. E. Leunissen *et al.*, Nature (London) **437**, 235 (2005).
[8] P. Poulin, H. Stark, T. C. Lubensky, and D. A. Weitz, Science **275**, 1770 (1997).
[9] I. Muševič, M. Škarabot, U. Tkalec, M. Ravnik, and S. Žumer, Science **313**, 954 (2006).
[10] Topological defects in a nematic liquid crystal are areas where the order parameter fields describing the molecular ordering are singular. A defect cannot be eliminated by a local continuous deformation of the nematic around the singularity. The formation of defects is a characteristic of symmetry breaking transitions.
[11] H. Stark, Phys. Rep. **351**, 387 (2001).
[12] T. C. Lubensky, D. Pettey, N. Currier, and H. Stark, Phys. Rev. E **57**, 610 (1998).
[13] S. Ramaswamy, R. Nityananda, V. A. Raghunathan, and J. Prost, Mol. Cryst. Liq. Cryst. **288**, 175 (1996).
[14] R. W. Ruhwandl and E. M. Terentjev, Phys. Rev. E **55**, 2958 (1997).
[15] O. Guzman, E. B. Kim, S. Grollau, N. L. Abbott, and J. J. de Pablo, Phys. Rev. Lett. **91**, 235507 (2003).
[16] S. Žumer, *21st International Liquid Crystal Conference, Keystone, Colorado, USA, July 2-7*, 2006.
[17] T. Araki and H. Tanaka Phys. Rev. Lett. **97**, 127801 (2006).
[18] M. Škarabot *et al.*, Phys. Rev. E **73**, 021705 (2006).
[19] E. B. Kim, O. Guzman, S. Grollau, N. L. Abbott, and J. J. de Pablo, J. Chem. Phys. **121**, 1949 (2004).
[20] P. G. de Gennes and J. Prost, *The Physics of Liquid Crystals* (Oxford Science, Oxford, 1993), 2nd ed.
[21] W. H. Press, B. P. Flannery, S. A. Teukolsky, and W. T. Vetterling, *Numerical Recipies* (Cambridge University Press, Cambridge, England, 1986).
[22] Jun-ichi Fukuda and H. Yokoyama, Phys. Rev. Lett. **94**, 148301 (2005).
[23] P. Poulin, V. Cabuil, and D. A. Weitz, Phys. Rev. Lett. **79**, 4862 (1997).
[24] The condensation of defect loops around colloidal particles in a homogenous planar layer reflects the topological restrictions on the formation of defect structures within the nematic layer, meaning that the net topological charge must be zero. Each colloidal particle, which is introduced into a homogeneous nematic, acts as a radial hedgehog, carrying a topological charge 1. As a result, the disclination lines are formed around particles, which must just compensate the net topological charge to zero. In the case of simple localized rings or intercalated point defects, each ring or point has a charge of 1. More complicated defect rings with a π-twist, such as the ''figure of eight'' carry the topological charge 2.
[25] M. Kleman and O. D. Lavrentovich, *Soft Matter Physics* (Springer-Verlag, New York, 2003).
[26] M. J. Bowick, L. Chandar, E. A. Schiff, and A. M. Srivastava, Science **263**, 943 (1994).
[27] C. J. Olson Reichhardt and M. B. Hastings, Phys. Rev. Lett. **92**, 157002 (2004).
[28] V. B. Eltsov, *et al.*, Phys. Rev. Lett. **96**, 215302 (2006).
[29] K. M. Benson and T. Imbo, Phys. Rev. D **70**, 025005 (2004).